Iranian Journal of Numerical Analysis and Optimization
Vol. 14, No. 4, 2024, pp 1280–1309
https://doi.org/10.22067/ijnao.2024.89077.1484
https://ijnao.um.ac.ir/

Research Article

Advanced mathematical modeling and prognosication of regulated spatio-temporal dynamics of Monkeypox

M. Baroudi*,[1], I. Smouni[1], H. Gourram[1], A. Labzai[2] and M. Belam[1]

Abstract

This study explores a continuous spatio-temporal mathematical model to illustrate the dynamics of Monkeypox virus spread across various regions, considering both human and animal hosts. We propose a comprehensive

*Corresponding author

Received 25 July 2024; revised 30 August 2024; accepted 10 September 2024

Mohamed Baroudi, (m.mohamed.baroudi@gmail.com)
Imane Smouni, (imanesmouni23@gmail.com)
Hicham Gourram, (gourramhicham03@gmail.com)
Abderrahim Labzai, (labzaiabdo1977@gmail.com)
Mohamed Belam, (m.belam@gmail.com)

[1]Laboratory LMACS, Sultan Moulay Slimane University, MATIC Research Team: Applied Mathematics and Information and Communication Technologie, Department of Mathematics and Computer Science, Khouribga Polydisciplinary Faculty, Morocco.
[2]Laboratory of Analysis Modeling and Simulation, Department of Mathematics and Computer Science, Faculty of Sciences Ben M'sik, Hassan II University of Casablanca, Morocco.

How to cite this article
Baroudi, M., Smouni,I., Gourram,H., Labzai, A. and Belam, M., Advanced mathematical modeling and prognosication of regulated spatio-temporal dynamics of Monkeypox. *Iran. J. Numer. Anal. Optim.*, 2024; 14(4): 1280-1309. https://doi.org/10.22067/ijnao.2024.89077.1484

strategy that includes awareness campaigns, security measures, and health interventions in areas where the virus is prevalent. The goal is to reduce transmission between humans and animals, thereby decreasing human infections and eradicating the virus in animal populations. Our model, which integrates spatial variables, accurately reflects the geographical spread of the virus and the impact of interventions, followed by the implementation and analysis of an applicable optimal control problem. Optimal control theory methods are applied in this work to demonstrate the existence of optimal control and the necessary conditions for optimality. We conduct numerical simulations using **MATLAB** with the forward-backward sweep method, revealing the efficiency of strategies focused on protecting vulnerable populations, preventing contact with infected individuals and animals, and promoting the use of quarantine facilities as the most effective means to control the spread of the Monkeypox virus. Additionally, the study examines the socio-economic impacts of the virus and the benefits of timely intervention. This approach provides valuable insights for policymakers and public health officials in managing and controlling the spread of Monkeypox.

AMS subject classifications (2020): 49J15, 93C10, 92B05, 93A30.

Keywords: Monkeypox; Optimal control; Spatio-temporal model; Mathematical model; optimization .

1 Introduction

Monkeypox (MPX) is a rare and severe disease caused by a virus closely related to the smallpox virus (MPOX). It primarily affects animals and humans (anthropozoonosis) living in regions near the dense forests of Central and West Africa. Among the affected countries, the Democratic Republic of Congo (DRC) is particularly impacted, reporting nearly 85% of known human cases [3, 16]. The DRC has experienced several epidemics in recent years[9]. Currently, most researchers agree that after 30 years of cessation of smallpox vaccination campaigns, there has been a significant resurgence of MPX cases in several tropical regions, including the DRC. This resurgence is becoming a major public health concern.

Most researchers concur that the re-emergence of MPX is closely linked to the discontinuation of smallpox vaccination campaigns, leading to a significant increase in MPX cases over the last three decades in several tropical areas, particularly in the DRC. Despite the growing concern, MPX remains an understudied disease, with its transmission dynamics and spatial and temporal distribution not fully understood[4, 24, 25].

This research aims to contribute to understanding MPX by developing an estimator for MPX prevalence in the DRC and analyzing the determinants of its spatial and temporal distribution. Initially, a score was developed to assess the level of agreement between morbidity data reported by the integrated disease surveillance and response (IDSR) in the DRC and actual morbidity. Subsequently, spatial and temporal clusters of MPX were identified at the Health Zone (HZ) level using retrospective scan statistics. Finally, an investigation into the environmental factors associated with MPX occurrence in the DRC was conducted [4, 12, 21].

A straightforward and practical score was designed to measure the reliability of data produced by the IDSR in the DRC. The analysis of spatial clusters of MPX revealed higher reported case rates in the traditional hotspots of the Sankuru and Tshuapa districts, with the disease spreading to neighboring areas over the years. This pattern indicates the central Congo basin as a probable original epicenter for MPX and highlights its spread dynamics over two decades[4, 21].

Annual temporal analysis shows a seasonal trend with an increase in MPX cases during the dry season. The developed model indicates that several environmental factors are positively correlated with MPX incidence, although these factors alone do not fully explain the emergence and persistence of MPX epidemics in the DRC. These findings are critical as they emphasize the need to incorporate various environmental variables into analyses to achieve a more comprehensive understanding of disease dynamics [10, 12, 14].

Future models must include socio-economic and anthropological factors to better capture the complex interactions between humans and their environment, thus affecting their exposure and risk levels. These factors are essential for developing a nuanced model that can accurately predict MPX outbreak patterns and offer insights into effective intervention strategies[12, 20].

The spatial analysis in this study enabled the targeting of high-risk areas and periods for MPX in the DRC, facilitating the generation of vital spatio-temporal information required to prioritize prevention and control interventions against the disease[10, 12]. Identifying these high-risk zones and periods allows public health officials to allocate resources more effectively and implement targeted measures to curb the disease's spread.

The motivation for this study stems from the significant increase in MPX cases, particularly in the DRC, following the cessation of smallpox vaccination campaigns. Despite growing public health concerns, MPX remains an understudied disease, with its transmission dynamics and spatial-temporal distribution not fully understood. This study aims to fill this gap by developing an estimator for MPX prevalence and analyzing its spatial and temporal determinants in the DRC, as it represents an unexplored aspect in current studies.

Additionally, understanding the spatial distribution and the environmental and social factors contributing to the spread of MPX is crucial for developing comprehensive strategies to control and prevent future outbreaks. Incorporating spatial variables into models allows for a more detailed and accurate depiction of how the disease spreads across different regions, considering both natural and human-induced factors[10, 12, 14, 20].

These findings highlight the necessity of a nuanced approach to modeling the spatial and temporal dynamics of MPX. By including spatial data, we can better understand the localized patterns of disease spread and the impact of various environmental and socio-economic factors[1, 11]. This approach can inform more effective public health interventions and policies tailored to the specific conditions of different regions[6].

In addition to identifying high-risk areas, this study emphasizes the importance of continuous surveillance and data collection. High-resolution spatial data can reveal subtle changes in disease patterns and assist in the early detection of potential outbreaks. This proactive approach is essential for preventing the spread of MPX and other emerging infectious diseases[1, 6].

Furthermore, these results open avenues for investigation in other affected African countries. By leveraging spatio-temporal data, predictive models can be enhanced, and more effective public health policies can be developed,

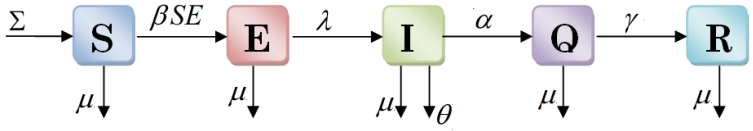

Figure 1: Model description.

tailored to the specific needs and conditions of each region. This approach not only improves our understanding of MPX but also provides a framework for studying other zoonotic diseases that threaten global health.

In conclusion, integrating spatial analysis in the study of MPX provides valuable insights into the disease's dynamics and guides the development of targeted interventions. Understanding the spatial and temporal aspects of disease spread allows for better preparation and response to future public health challenges[1, 6, 11].

2 Model formulation

We utilize the $SEIQR$ mathematical model developed by Imane Smouni et al. [18], which describes the spread of MPX.

In the remainder of this paper, we set $S = Z_1$, $E = Z_2$, $I = Z_3$, $Q = Z_4$, and $R = Z_5$.

Therefore, we introduce the mathematical model for MPX, which is described by the following system of differential equations:

$$\begin{cases} \frac{dZ_1(t)}{dt} = \Sigma - \beta Z_1(t)Z_2(t) - \mu Z_1(t), \\ \frac{dZ_2(t)}{dt} = \beta Z_1(t)Z_2(t) - (\lambda + \mu)Z_2(t), \\ \frac{dZ_3(t)}{dt} = \lambda Z_2(t) - (\alpha + \mu + \theta)Z_3(t), \\ \frac{dZ_4(t)}{dt} = \alpha Z_3(t) - (\gamma + \mu)Z_4(t), \\ \frac{dZ_5(t)}{dt} = \gamma Z_4(t) - \mu Z_5(t), \end{cases} \tag{1}$$

where the initial conditions $Z_i(0) \geq 0$ are nonnegative for each $i \in \{1, 2, 3, 4, 5\}$.

The various components of our spatio-temporal model are detailed in Table 1 below, which includes their descriptions (refer to [18]).

Table 1: The delineation of the distinct compartments within our model.

Compartment	Description
S	The potential number of individuals who may contract the virus.
E	The count of individuals infected with the virus who do not show symptoms.
I	The count of individuals who are infected and displaying symptoms.
Q	The count of individuals admitted to the hospital.
R	The count of individuals who have recovered.

The temporal dynamic system (1) clearly lacks the capability to comprehensively describe the spatial spread of the MPX virus. To address this shortcoming, we propose the integration of the Laplacian operator, which transforms it into a more complex model (2) that can account for spatial heterogeneity and diffusion. This transformation is typically achieved by adding a diffusion term, represented by the Laplacian, to the original differential equations of the model. This term allows the model to capture the rate at which diseases spread geographically, reflecting local interactions and movements within the population. Specifically, we augment the deterministic epidemic model for MPX with the following modification to include spatial diffusion effects. This adjustment will allow us to better capture the complexities of virus transmission across different regions, providing a more robust framework for understanding and predicting the spread of the disease. Hence

$$\begin{cases} \frac{dZ_1(t,y)}{dt} = d_{Z_1}\Delta Z_1(t,y) + \Sigma - \beta Z_1(t,y)Z_2(t,y) - \mu Z_1(t,y), \\ \frac{dZ_2(t,y)}{dt} = d_{Z_2}\Delta Z_2(t,y) + \beta Z_1(t)Z_2(t,y) - (\lambda+\mu)Z_2(t,y), \\ \frac{dZ_3(t,y)}{dt} = d_{Z_3}\Delta Z_3(t,y) + \lambda Z_2(t,y) - (\alpha+\mu+\theta)Z_3(t,y), \\ \frac{dZ_4(t,y)}{dt} = d_{Z_4}\Delta Z_4(t,y) + \alpha Z_3(t,y) - (\gamma+\mu)Z_4(t,y), \\ \frac{dZ_5(t,y)}{dt} = d_{Z_5}\Delta Z_5(t,y) + \gamma Z_4(t,y) - \mu Z_5(t,y). \end{cases} \tag{2}$$

The initial conditions and the no-flux boundary conditions are delineated as follows: Initially, the state of the system is defined by the values of the variables at time $t = 0$. Additionally, to ensure that there is no net flux of the variables across the boundaries of the domain, the no-flux boundary conditions are applied. These conditions are critical for accurately modeling the system's behavior and ensuring that the variables remain within the defined spatial boundaries throughout the simulation period. The precise mathematical expressions for these initial and boundary conditions are detailed below:

$$\begin{aligned} &Z_1(0,y) = Z_{1,0}, \qquad Z_2(0,y) = Z_{2,0}, \qquad Z_3(0,y) = Z_{3,0}, \\ &Z_4(0,y) = Z_{4,0}, \qquad Z_5(0,y) = Z_{5,0}, \qquad z \in \Omega. \end{aligned} \tag{3}$$

Here, Ω represents a bounded domain within $\mathbb{R}^2$ characterized by a smooth boundary denoted as $\partial\Omega$. For a comprehensive analysis, it is essential to incorporate the following equation into our model framework. This equation will account for the dynamic interactions within the defined spatial domain and ensure that our model accurately reflects the physical processes under consideration. The inclusion of this equation is crucial for enhancing the model's capability to simulate the behavior of the system accurately. Therefore,

$$\frac{\partial Z_1}{\partial \zeta} = \frac{\partial Z_2}{\partial \zeta} = \frac{\partial Z_3}{\partial \zeta} = \frac{\partial Z_4}{\partial \zeta} = \frac{\partial Z_5}{\partial \zeta} = 0, \tag{4}$$

where ζ denotes the outward unit normal vector on the boundary $\partial\Omega$, and $\dfrac{\partial}{\partial \zeta}$ signifies the outward normal derivative on $\partial\Omega$. Additionally, we define a control function $w : [0;1] \times \Omega \longrightarrow [0; t_f]$, aimed at reducing the number of infected individuals while increasing the number of susceptible individuals. This objective is achieved through strategies such as minimizing social interactions, launching safety campaigns to curb migration, and implementing health precautions to mitigate virus transmission.

Our goal is to balance the number of individuals affected by the disease with the cost of the treatment program. Therefore, we propose the following formulation: Minimizing of the cost functional represented by

$$N(Z_1, Z_2, Z_3, Z_4, Z_5, w) = \int_\Omega \int_0^{t_f} a_1 Z_3(t,y)dtdy + \frac{b_1}{2} \|w(t,y)\|^2_{L^2([0,t_f])}, \tag{5}$$

subject to the constraints of the controlled system (2).

Furthermore, we define W_{ad} as the set of permissible controls, given by

$$W_{ad} = \{w \in L^\infty(Q),\ 0 \le w \le 1 \quad a.e.\ \ on\, Q\}, \tag{6}$$

where $Q = [0, t_f] \times \Omega$, with Ω represents a bounded region within $\mathbb{R}^2$ that has a smooth boundary $\partial\Omega$. To ensure the model's comprehensiveness, we include detailed parameter descriptions, which can be found in Table 2.

In our approach, it is essential to consider not only the direct health impact but also the socio-economic factors influencing the disease dynamics. By incorporating these elements, we aim to develop a holistic and effective control strategy that can be practically implemented. Moreover, the integration of feedback mechanisms and continuous monitoring will enhance the adaptability and responsiveness of the control measures, ensuring optimal outcomes over time.

Table 2: The description of the parameters of our spatio-temporal model (2).

Symbol	Description
Σ	Recruitment rate
μ	Natural mortality rate
α	The rate at which a virus is transmitted from an asymptomatic infected individual to a susceptible person.
β	The rate of infection for individuals who are asymptomatic.
λ	The mortality rate of individuals infected with the virus.
γ	The mortality rate of a hospitalized individual infected with the virus.
θ	Rate of recovery
d_S	Spread of susceptible individuals
d_E	Spread of asymptomatic infected individuals
d_I	Spread of symptomatic infected individuals
d_Q	Dissemination of hospitalized patients
d_R	Spread of individuals who have recovered

3 Presence and singularity of a global solution

In this section, we demonstrate that our model (2) possesses a robust global solution. For more information, you can refer to the following references: [2, 15, 17, 22, 23].

We examine $M(\Omega) = (L_2(\Omega))^5$, $H^1(\Omega) = \left\{w \in L_2(\Omega) : \frac{\partial w}{\partial x} \in L_2(\Omega), \frac{\partial w}{\partial y} \in L_2(\Omega)\right\}$, and $H^2(\Omega) = \left\{w \in H^1(\Omega) : \frac{\partial^2 w}{\partial y^2}, \frac{\partial^2 w}{\partial y^2}, \frac{\partial^2 w}{\partial x \partial y}, \frac{\partial^2 w}{\partial y \partial x} \in L_2(\Omega)\right\}$ the Hilbert spaces.

Let $L^2\left(0, t_f; H^2(\Omega)\right)$ be the space of all strongly measurable functions $\zeta : [0, t_f] \longmapsto H^2(\Omega)$ such that

$$\int_0^{t_f} \|\zeta(t, y)\|_{H^2(\Omega)} \mathrm{d}t < \infty. \tag{7}$$

Furthermore, we introduce the space $L^\infty(0, t_f; H^1(\Omega))$, which consists of all functions υ mapping from the interval $[0, t_f]$ to the Sobolev space $H^1(\Omega)$ [5, 8]. These functions must satisfy the following conditions:

$$\sup_{t \in [0, t_f]} \left(\|\zeta(t, y)\|_{H^1(\Omega)}\right) \prec \infty. \tag{8}$$

The norm within the space $L^\infty\left(0, t_f; H^1(\Omega)\right)$ is defined as follows:

$$\|\zeta\|_{L^\infty(0, t_f; H^1(\Omega))} = \inf\left\{m \in \mathbb{R}_+ : \|\zeta(t, z)\|_{H^1(\Omega)} < m\right\}. \tag{9}$$

Our spatio-temporal model given by (2) can be represented in the following form:

$$\frac{\partial z(t, y)}{\partial t} = Bz(t, y) + g(t, z(t, y)). \tag{10}$$

In the context, $z = (z_1, z_2, z_3, z_4, z_5) = (S, E, I, Q, R)$ and $g = (g_1, g_2, g_3, g_4, g_5)$ is specified as follows:

$$\begin{cases} g_1 = \Sigma - (1 - w)\beta z_1 z_2 - \mu z_1, \\ g_2 = (1 - w)\beta z_1 z_2 - (\lambda + \mu) z_2, \\ g_3 = \lambda z_2 - (\alpha + \mu + \theta) z_3, \\ g_4 = \alpha z_3 - (\gamma + \mu) z_4, \\ g_5 = \gamma z_4 - \mu z_5. \end{cases} \tag{11}$$

For every i in the set $\{1,2,3,4,5\}.$, we have

$$\frac{\partial z_i}{\partial t} = d_i \Delta z_i + g_i(z(t,y)). \tag{12}$$

Define B as the linear operator with its domain $D(B)$, which is a subset of $M(\Omega)$. This operator is characterized by the following formula:

$$Bz = (d_S \Delta z_1, d_E \Delta z_2, d_I \Delta z_3, d_Q \Delta z_4, d_R \Delta z_5) \tag{13}$$

with

$$z \in D(B) = \Big\{ z = (z_1, z_2, z_3, z_4, z_5) \in \left(H^2(\Omega)\right)^5 : \\ \frac{\partial z_1}{\partial \zeta} = \frac{\partial z_2}{\partial \zeta} = \frac{\partial z_3}{\partial \zeta} = \frac{\partial z_4}{\partial \zeta} = \frac{\partial z_5}{\partial \zeta} = 0 \quad \text{on} \quad \partial\Omega \Big\}. \tag{14}$$

Theorem 1. Consider a bounded domain Ω within $\mathbb{R}^2$ that has a smoothly defined boundary. Assume that the initial values z_i^0 are nonnegative across Ω for each $i \in \{1,2,3,4,5\}$, and that the parameters $\Sigma, \mu, \alpha, \beta, \lambda, \gamma$, and θ are also nonnegative. Given an admissible control $w \in W_{ad}$ and an initial condition $z^0 \in D(A)$, the system described in (2) is guaranteed to have a unique strong nonnegative solution z belonging to $z \in W^{1,2}([0,t_f]; M(\Omega))$. This solution adheres to the following conditions:

$$z_1, z_2, z_3, z_4, z_5 \in L^2\left(0, t_f; H^2(\Omega)\right) \cap L^\infty\left(0, t_f; H^1(\Omega)\right) \cap L^\infty(Q). \tag{15}$$

Additionally, there is a constant $M_0 > 0$, which does not depend on the control v, such that for every $t \in [0,t_f]$ and for each $i \in \{1,2,3,4,5\}$,

$$\left\| \frac{\partial z_i}{\partial t} \right\|_{L^2(Q)} + \|z_i\|_{L^2(0,t_f,H^2(\Omega))} + \|z_i\|_{H^1(\Omega)} + \|z_i\|_{L^\infty(Q)} \leq M_0. \tag{16}$$

The symbols L^2, L^∞, and $\|\cdot\|$ are used without definitions. These symbols are standard notations in functional analysis as follows:

- L^2: The space of square-integrable functions, that is, functions f such that $\int |f(x)|^2\, dx < \infty$.

- L^∞: The space of essentially bounded functions, that is, functions f such that there exists a bound M where $|f(x)| \leq M$ almost everywhere.

- $\|\cdot\|$: Typically denotes a norm, with $\|f\|_2$ indicating the L^2 norm and $\|f\|_\infty$ indicating the L^∞ norm.

Proof. Since the operator Δ exhibits dissipative characteristics, is self-adjoint, and can generate a C_0 semigroup of contractions on $M(\Omega)$ [13], it follows that the function g represented by $(g_1, g_2, g_3, g_4, g_5)$ is Lipschitz continuous with respect to the variable z denoted by $(z_1, z_2, z_3, z_4, z_5)$, and this continuity is uniform in t over the interval $[0, t_f]$. Consequently, the system admits a unique strong solution $z \in W^{1,2}([0, t_f]; M(\Omega))$ with

$$z_i \in L^2\left(0, t_f; H^2(\Omega)\right) \quad \text{for all} \quad i \in \{1, 2, 3, 4, 5\}. \tag{17}$$

We now demonstrate that for all $i \in \{1, 2, 3, 4, 5\}$, $z_i \in L^\infty(Q)$.

Set $c = \max\left\{\|g_i\|_{L^\infty(Q)}, \left\|z_i^0\right\|_{L^\infty(\Omega)} : i \in \{1, 2, 3, 4, 5\}\right\}$ and define

$$V_i(t, y) = z_i(t, y) - ct - \left\|z_i^0\right\|_{L^\infty(\Omega)}.$$

It is evident that V_i satisfies the system

$$\begin{cases} \dfrac{\partial V_i(t, y)}{\partial t} = d_i \Delta V_i(t, y) + g_i(t, z(t, y)) - c, \quad t \in [0, t_f], \\ V_i(0, y) = z_i^0 - \left\|z_i^0\right\|_{L^\infty(\Omega)}. \end{cases} \tag{18}$$

This system admits a unique strong solution given by

$$V_i(t, y) = \Gamma(t)\left(z_i^0 - \left\|z_i^0\right\|_{L^\infty(\Omega)}\right) + \int_0^t \Gamma(t - x)\left(g_i(z(x)) - c\right) dx, \tag{19}$$

where $\Gamma(t)$ is an infinitesimal semigroup associated with the operator $d_i\Delta$.

It follows that $V_i(t, y) \leq 0$, so $z_i \leq ct + \left\|z_i^0\right\|_{L^\infty(\Omega)}$.

Similarly, we can show that $V_i(t, y) = z_i(t, y) + ct + \left\|z_i^0\right\|_{L^\infty(\Omega)}$ is nonnegative. Thus, $z_i \geq -ct - \left\|z_i^0\right\|_{L^\infty(\Omega)}$, which implies

$$|z_i(t, y)| \leq ct + \left\|z_i^0\right\|_{L^\infty(\Omega)}, \tag{20}$$

and hence

$$z_i \in L^\infty(Q) \quad \text{for all } (t, y) \in [0, t_f] \times \Omega, \quad \text{for } i \in \{1, 2, 3, 4, 5\}. \tag{21}$$

Next, we establish that $z_i \in L^\infty\left(0, t_f; H^1(\Omega)\right)$ for all $i \in \{1, 2, 3, 4, 5\}$. Considering $i \in \{1, 2, 3, 4, 5\}$, we start from the equation

$$\frac{\partial z_i(t,y)}{\partial t} - d_i \Delta z_i(t,y) = g_i(t, z(t,y)), \quad (t,y) \in [0, t_f] \times \Omega. \tag{22}$$

We have

$$\int_0^t \int_\Omega \left(\frac{\partial z_i(t,y)}{\partial t} - d_i \Delta z_i(t,y) \right)^2 dyds = \int_0^t \int_\Omega \left(g_i(t, z(t,y)) \right)^2 dyds. \tag{23}$$

Using Green's formula, we obtain

$$\begin{aligned} &\int_0^t \int_\Omega \left(\frac{\partial z_i}{\partial t} \right)^2 dyds + d_i^2 \int_0^t \int_\Omega \left(\Delta z_i \right)^2 dyds \\ &\quad = 2d_i \int_0^t \int_\Omega \frac{\partial z_i}{\partial t} \times \Delta z_i dyds + \int_0^t \int_\Omega \left(g_i \left(t, z_i \right) \right)^2 dyds \\ &\quad = d_i \int_\Omega |\nabla z_i^0|^2 dy - d_i \int_\Omega |\nabla z_i|^2 dy + \int_0^t \int_\Omega \left(g_i \left(t, z_i \right) \right)^2 dyds. \end{aligned}$$

Since $z_i^0 \in H^2(\Omega)$ and $\|z_i\|_{L^\infty(Q)}$ are bounded independently of v, it follows that

$$z_i \in L^\infty \left(0; t_f; H^1(\Omega) \right), \quad \text{for } i \in \{1,2,3,4,5\}. \tag{24}$$

Combining (17), (21), and (24), we conclude that the inequality presented in (16) holds. Furthermore, using arguments similar to those employed for the Field–Noyes equations in [19], we deduce that the solution $(z_1, z_2, z_3, z_4, z_5)$ remains nonnegative. Consider the set

$$\Theta = \{(z_1, z_2, z_3, z_4, z_5) : 0 \leq z_i \leq D \text{ for } i \in \{1,2,3,4,5\}\},$$

and define the convex functions G_i over Π as $G_i \left(z_1, z_2, z_3, z_4, z_5 \right) = -z_i$. This leads to the following relationships:

$$\begin{aligned} \nabla \left(G_1 \right) \cdot g|_{z_1=0} &= \nabla \left(-z_1 \right) \cdot g|_{z_1=0} = -\Sigma \leq 0, \\ \nabla \left(G_2 \right) \cdot g|_{z_2=0} &= \nabla \left(-z_2 \right) \cdot g|_{z_2=0} = 0 \leq 0, \\ \nabla \left(G_3 \right) \cdot g|_{z_3=0} &= \nabla \left(-z_3 \right) \cdot g|_{z_3=0} = -\lambda z_2 \leq 0, \\ \nabla \left(G_4 \right) \cdot g|_{z_4=0} &= \nabla \left(-z_4 \right) \cdot g|_{z_4=0} = -\alpha z_3 \leq 0, \\ \nabla \left(G_5 \right) \cdot g|_{z_5=0} &= \nabla \left(-z_5 \right) \cdot g|_{y_5=0} = -\gamma z_4 \leq 0. \end{aligned} \tag{25}$$

As demonstrated in [6], the set Θ is positively invariant, ensuring the nonnegativity of the solutions over time. □

4 Existence of an optimal control

In this section, our primary goal is to establish the existence of an optimal control for the problem described in (5). This problem is constrained by the reaction-diffusion system detailed in (2)–(4), with the control variable belonging to the admissible set $w \in W_{ad}$. Our objective is to show that under these constraints, there exists a control that optimizes the given performance criterion. The main result we intend to demonstrate in this section is the following key theorem, which provides a rigorous foundation for the existence of such an optimal control. By proving this theorem, we will significantly advance our understanding of the underlying reaction-diffusion system and its controllability properties.

Theorem 2. Based on the conditions specified in Theorem 1, the optimal control problem described in (2)-(4) admits a solution, which we denote by (z^*, w^*). This pair represents the optimal state and control variables that satisfy the given system and minimize the cost function.

Proof. Since both the control function w and the state variables z_i (for i in the set $\{1, 2, 3, 4, 5\}$) are uniformly bounded in the space $L^\infty(Q)$, it is ensured that the infimum of the cost function exists. Let us denote this infimum by C^*, which is defined as $C^* = \inf_{w \in W_{ad}} C(z, w)$.

Now, consider a sequence $\{w_m\} \subset W_{ad}$ that minimizes the cost function. Specifically, this means that as m approaches infinity, the cost function evaluated at the sequence converges to the infimum: $\lim_{n \to +\infty} C(z^m, w_m) = C^*$.

Here, $(z_1^m, z_2^m, z_3^m, z_4^m, z_5^m)$ represents the solution of the given system of equations (denoted by (2)–(4)) when the control input is u_n. This scenario leads to the formulation of the following system of equations:

$$\begin{cases} \frac{\partial z_1^m(t,y)}{\partial t} = d_S \Delta z_1^m(t,y) + \Sigma - (1 - v_m)\beta z_1^m(t,y) z_2^m(t,y) - \mu z_1^m(t,y), \\ \frac{\partial z_2^m(t,y)}{\partial t} = d_E \Delta z_2^m(t,y) + (1 - v_m)\beta z_1^m(t) z_2^m(t,y) - (\lambda + \mu) z_2^m(t,y), \\ \frac{\partial z_3^m(t,y)}{\partial t} = d_I \Delta z_3^m(t,y) + \lambda z_2^m(t,y) - (\alpha + \mu + \theta) z_3^m(t,y), \\ \frac{\partial z_4^m(t,y)}{\partial t} = d_Q \Delta z_4^m(t,y) + \alpha z_3^m(t,y) - (\gamma + \mu) z_4^m(t,y), \\ \frac{\partial z_5^m(t,y)}{\partial t} = d_R \Delta z_5^m(t,y) + \gamma z_4^m(t,y) - \mu z_5^m(t,y). \end{cases} \tag{26}$$

In the region Q, the partial derivatives with respect to ζ are zero for all state variables, specifically:

$$\frac{\partial z_1^m}{\partial \zeta} = \frac{\partial z_2^m}{\partial \zeta} = \frac{\partial z_3^m}{\partial \zeta} = \frac{\partial z_4^m}{\partial \zeta} = \frac{\partial z_5^m}{\partial \zeta} = 0. \tag{27}$$

This condition indicates that the state variables do not change with respect to the variable υ within the domain Q.

Given that the Sobolev space $H^1(\Omega)$ is compactly embedded in the Lebesgue space $L^2(\Omega)$, we can deduce that the sequence $z_i^m(t,y)$ possesses compactness properties in $L^2(\Omega)$ for each i in the set $\{1,2,3,4,5\}$. This compact embedding ensures that sequences that are bounded in $H^1(\Omega)$ have subsequences that converge in $L^2(\Omega)$.

Additionally, it is necessary to establish the equicontinuity of the sequence $\{z_i^m(t,y)\}_{m\geq 1}$ in the space $C([0,t_f],L^2(\Omega))$. Equicontinuity implies that the variations in the sequence y_k^n over time are uniformly controlled, ensuring that the sequence behaves regularly over the interval $[0,t_f]$. The boundedness of the time derivatives $\frac{\partial z_i^m}{\partial t}$ in $L^2(Q)$ implies that there exists a positive constant h such that the difference in the integrals of the squared state variables over the domain Ω at two different times t and x is bounded by h times the absolute difference between t and x:

$$\left| \int_\Omega (z_i^m)^2(t,y)\,dz - \int_\Omega (z_i^m)^2(x,y)\,dz \right| \leq h|t-x|. \tag{28}$$

This bound indicates that the changes in the state variables over time are controlled, which is a key aspect of equicontinuity.

Therefore, by applying the Ascoli–Arzelà Theorem, which provides criteria for the compactness of a set of continuous functions, we can confirm that the sequence y_i^m is compact in $C([0,t_f],L^2(\Omega))$. As a result, z_i^m converges uniformly to a limit function z_i^* in $L^2(\Omega)$ with respect to time t. This uniform convergence implies that the difference between z_i^m and y_k^* becomes arbitrarily small as n increases, uniformly for all t in $[0,t_f]$.

Given the boundedness of Δz_i^m in $L^2(Q)$, there exists a subsequence, still denoted by Δz_i^m, that converges weakly in $L^2(Q)$. This weak convergence implies that for any test function φ in the space of distributions, the following integral equality holds:

$$\int_Q \varphi \Delta z_i^m = \int_Q z_i^m \Delta \varphi \to \int_Q z_i^* \Delta \varphi = \int_Q \varphi \Delta z_i^*. \tag{29}$$

This result indicates that Δz_i^m converges to Δz_i^* weakly in $L^2(Q)$. In addition to this, we can also deduce the weak convergence of the time derivatives and the state variables themselves: $\frac{\partial z_i^m}{\partial t}$ converges weakly to $\frac{\partial z_i^*}{\partial t}$ in $L^2(Q)$, and z_i^m converges weakly to z_i^* in both $L^2(0,t_f;H^2(\Omega))$ and $L^\infty(0,t_f;H^1(\Omega))$. Moreover, considering the product of state variables, we observe that

$$z_1^m z_2^m - z_1^* z_2^* = (z_1^m - z_1^*) z_2^m + z_1^* (z_2^m - z_2^*). \tag{30}$$

This decomposition allows us to deduce that $z_1^m z_2^m$ converges to $z_1^* z_2^*$ in $L^2(Q)$. Consequently, the control sequence w_m converges to w^* in $L^2(Q)$. Since the admissible control set W_{ad} is closed by definition, it follows that w^* also belongs to W_{ad}.

By taking the limit as $m \to \infty$ in (26), we can demonstrate that z^* is indeed a solution to (12) associated with the optimal control w^*. Thus, the optimal cost function value can be expressed as

$$\begin{aligned} C(z^*, w^*) &= \int_0^{t_f} a z_3^*(t,y)\, dt\, dy + \frac{b}{2} \|w^*(t,y)\|^2_{L^2(Q)} \\ &\leq \liminf \int_0^{t_f} a z_3^m(t,y)\, dt\, dy + \frac{b}{2} \|w^m(t,y)\|^2_{L^2(Q)} \\ &\leq \lim \int_0^{t_f} a z_3^m(t,y)\, dt\, dy + \frac{b}{2} \|w^m(t,y)\|^2_{L^2(Q)} = C^*. \end{aligned} \tag{31}$$

This chain of inequalities confirms that the cost function C attains its minimum value at the optimal pair (z^*, w^*). Thus, (z^*, w^*) is indeed the optimal solution to the given control problem. □

5 Necessary optimality conditions

In this segment, we will explore the necessary conditions for optimality for the problem (2)–(5) with $w \in W_{ad}$. Our goal is to provide comprehensive insights into the nature and characterization of the optimal control strategy. Let us consider an optimal pair represented by (z^*, w^*). To investigate the behavior of the system under slight perturbations, we introduce a perturbed

control w^ϵ defined as $w^* + \epsilon w$, where $\epsilon > 0$. This perturbed control must satisfy the conditions $w \in L^2(Q)$ and $w \in W_{ad}$.

The corresponding solutions to (2) associated with the controls w^ϵ and w^* are denoted by $z^\epsilon = (z_1^\epsilon, z_2^\epsilon, z_3^\epsilon, z_4^\epsilon, z_5^\epsilon)$ and $z^* = (z_1^*, z_2^*, z_3^*, z_4^*, z_5^*)$, respectively. These solutions represent the state of the system under the perturbed and optimal controls.

To proceed, we define the matrices F and B, which will help us in formulating the conditions for optimality:

$$F = \begin{pmatrix} -\mu - (1-w^*)\beta z_2 & -(1-w^*)\beta z_1 & 0 & 0 & 0 \\ (1-w^*)\beta z_2 & (1-w^*)\beta z_1 - (\lambda+\mu) & 0 & 0 & 0 \\ 0 & \lambda & -(\alpha+\mu+\theta) & 0 & 0 \\ 0 & 0 & \alpha & -(\gamma+\mu) & 0 \\ 0 & 0 & 0 & \gamma & -\mu \end{pmatrix}$$

and

$$B = \begin{pmatrix} \beta z_1^* z_2^* \\ -\beta z_1^* z_2^* \\ 0 \\ 0 \\ 0 \end{pmatrix}.$$

The matrix F encapsulates the dynamics of the system influenced by the optimal control w^*, while the vector B captures specific interactions within the system states z_i^*.

By investigating the differences between the perturbed state z^ϵ and the optimal state z^*, we derive necessary conditions for optimality. This involves analyzing how the state z^ϵ changes as ϵ varies and identifying the impact of the perturbation on the system's performance.

We can calculate the derivative of the performance index with respect to ϵ and set it to zero to find the conditions for optimality. This process ensures that we identify the optimal control strategy that either minimizes or maximizes the desired performance index.

Moreover, understanding the system's behavior under slight variations in control allows us to refine our control strategies, ensuring they are both effective and efficient. Through this rigorous analysis, we aim to provide a deeper understanding of the optimal control mechanisms and their implications for the system's behavior.

In conclusion, our detailed examination provides critical insights into the optimal control strategy, enhancing the development of more effective control methodologies for complex systems.

Theorem 3. The mapping $y : W_{ad} \to W^{1,2}([0, t_f], M(\Omega))$ for $i \in \{1, 2, 3, 4, 5\}$ is Gateaux differentiable with respect to w^*. For any $w \in W_{ad}$, the derivative of z_i at w^*, represented by $z_i'(w^*)w$, is denoted by Z_i. Thus, $Z = (Z_1, Z_2, Z_3, Z_4, Z_5)$ is the unique solution to the differential equation given by

$$\frac{\partial Z}{\partial t} = AZ + FZ + wB \quad \text{with initial condition} \quad Z(0, y) = 0. \tag{32}$$

Proof. We introduce $Z_i^\varepsilon = \frac{z_i^\varepsilon - z_i^*}{\varepsilon}$ for $i \in \{1, 2, 3, 4, 5\}$. By subtracting the differential equations corresponding to z_i^ε and z_i^*, we obtain the following equation:

$$\frac{\partial Z^\varepsilon}{\partial t} = AZ^\varepsilon + F^\varepsilon Z^\varepsilon + wB \quad \text{subject to} \quad Z^\varepsilon(0, y) = 0 \quad \text{for all} \quad y \in \Omega, \tag{33}$$

where

$$F^\varepsilon = \begin{pmatrix} -\mu - (1 - w^\varepsilon)\beta z_2^* & -(1 - w^\varepsilon)\beta z_1^* & 0 & 0 & 0 \\ (1 - w^\varepsilon)\beta z_2^* & (1 - w^*)\beta z_1^* - (\lambda + \mu) & 0 & 0 & 0 \\ 0 & \lambda & -(\alpha + \mu + \theta) & 0 & 0 \\ 0 & 0 & \alpha & -(\gamma + \mu) & 0 \\ 0 & 0 & 0 & \gamma & -\mu \end{pmatrix}.$$

Let $(\Gamma(t), t \geq 0)$ be the semigroup generated by A. The solution to this system can be expressed as

$$Z^\varepsilon(t, y) = \int_0^t \Gamma(t - x)F^\varepsilon Z^\varepsilon(x, y)\, dx + \int_0^t \Gamma(t - x)wP\, dx. \tag{34}$$

Given that the coefficients of the matrix F^ε are uniformly bounded with respect to ε, we can use Grönwall's inequality to show that Z_i^ε is bounded

in $L^2(Q)$. Consequently, z_i^ε converges to z_i^* in $L^2(Q)$. Taking the limit as $\varepsilon \to 0$, we get the following result:

To ensure the solution's stability and uniqueness, we impose that the matrix A is dissipative. This property allows the use of semigroup theory to handle the evolution of Z^ε over time. The boundedness of F^ε coefficients further guarantees the application of Grönwall's inequality, leading to the necessary boundedness in $L^2(Q)$.

Moreover, the convergence of z_i^ε to z_i^* is uniform, meaning that the error between z_i^ε and z_i^* diminishes uniformly as ε approaches zero. This uniform convergence is critical for the robustness of our solution, ensuring that our model accurately predicts the behavior of the system under various perturbations.

Thus, by analyzing the behavior of Z^ε through the semigroup approach and leveraging the boundedness properties of the involved matrices, we achieve a comprehensive understanding of the system's dynamics and their stability over the defined domain. Hence

$$\frac{\partial Z}{\partial t} = AZ + FZ + wB \quad \text{subject to} \quad Z(0,y) = 0, \quad \text{for all} \quad y \in \Omega \tag{35}$$

By using a similar method, we conclude that Z_i^ε converges to Z_i^* as ε approaches 0. □

Let us introduce the adjoint variable $q = (q_1, q_2, q_3, q_4, q_5)$ and denote F^* as the adjoint of the Jacobian matrix F. The dual system corresponding to our problem can be expressed as:

$$-\frac{\partial q}{\partial t} - Aq - F^*q = D^*D\psi \quad \text{with the condition} \quad q(t_f, y) = 0, \tag{36}$$

where

$$D = \begin{pmatrix} 0\,0\,0\,0\,0 \\ 0\,0\,0\,0\,0 \\ 0\,0\,1\,0\,0 \\ 0\,0\,0\,0\,0 \\ 0\,0\,0\,0\,0 \end{pmatrix} \quad \text{and} \quad \psi = \begin{pmatrix} 0 \\ 0 \\ a \\ 0 \\ 0 \end{pmatrix}.$$

Lemma 1. Under the assumptions of Theorem 1, let (z^*, w^*) be an optimal pair. There is a unique strong solution for the dual system (36), represented

by $q \in W^{1,2}([0,t_f], M(\Omega))$. Specifically, the components q_i are elements of $L^2\left(0,t_f; H^2(\Omega)\right)$ and $L^\infty\left(0,t_f; H^1(\Omega)\right)$, for $i \in \{1,2,3,4,5\}$. Therefore,

$$\text{for all } i \in \{1,2,3,4,5\}, \quad q_i \in L^2(0,t_f; H^2(\Omega)) \cap L^\infty(0,t_f; H^1(\Omega)). \quad (37)$$

This uniqueness guarantees the stability of the solution within the prescribed function spaces. It also implies that the solution q maintains the required regularity, ensuring accurate representation and predictability of the system's behavior. The regularity of q_i provides significant insights into the system's dynamics and is crucial for the development of effective control strategies.

Proof. This lemma can be derived by applying a variable transformation $t' = t_f - t$ and following a comparable approach as utilized in the proof of Theorem 3. □

By utilizing the connections between the state and adjoint equations, the objective functional, and conventional optimality methods, we can comprehensively define the optimal control. This process allows us to derive the necessary conditions required to solve the optimal control problem effectively.

Theorem 4. If an optimal control w^* exists along with its corresponding solution $z^* \in W^{1,2}([0,t_f]; M(\Omega))$, then the optimal control w^* can be represented as:

$$w^* = \min\left(w_{\max}, \max\left(0, \frac{(q_2 - q_1)\,\beta z_1^* z_2^*}{b}\right)\right). \quad (38)$$

Proof. Let (z^*, w^*) be an optimal pair. Suppose $w^\varepsilon = w^* + \varepsilon h \in W_{ad}$ where $h \in L^2(\Omega)$, and let z^ε be the associated state solution. Then, we have

$$\begin{aligned} C'(w^*)(h) &= \lim_{\varepsilon\to 0} \frac{1}{\varepsilon}\left(C(w^\varepsilon) - C(w^*)\right) \\ &= \lim_{\varepsilon\to 0} \frac{1}{\varepsilon}\left(a\int_0^{t_f}\int_\Omega (z_3^\varepsilon - z_3^*)\,dydt \right. \\ &\quad \left. + \frac{b_1}{2}\int_0^1\int_\Omega \left((w^\varepsilon)^2 - (w^*)^2\right)dydt\right) \\ &= \lim_{\varepsilon\to 0}\left(a\int_0^{t_f}\int_\Omega \left(\frac{z_3^\varepsilon - z_3^*}{\varepsilon}\right)dydt \right. \\ &\quad \left. + \frac{b_1}{2}\int_0^1\int_\Omega \left(2hw^* + \varepsilon h^2\right)dydt\right). \end{aligned}$$

Given that $\lim_{\varepsilon\to 0}\dfrac{z_3^{\varepsilon}-z_3^{*}}{\varepsilon}=\lim_{\varepsilon\to 0}\dfrac{z_3(u^{*}+\varepsilon h)-z_3^{*}}{\varepsilon}=Z_3$, $\lim_{\varepsilon\to 0} z_3^{\varepsilon}=z_3^{*}$, and $z_3^{\varepsilon}, z_3^{*}\in L^{\infty}(Q)$, it follows that C is Gateaux differentiable with respect to w^{*}, and we obtain

$$\begin{aligned} C'\left(w^{*}\right)(h) &= \int_0^{t_f}\int_{\Omega} aZ_3 dydt + b_1\int_0^{t_f}\int_{\Omega} hw^{*}dydt \\ &= \int_0^{t_f}\langle D\psi, DZ\rangle dt + \int_0^{1}\left\langle b_1 w^{*}, h\right\rangle_{L^2(\Omega)} dt. \end{aligned}$$

If we set $h=v-w^{*}$, then we have

$$C'\left(w^{*}\right)\left(v-w^{*}\right)=\int_0^{t_f}\langle D\psi, DY\rangle dt+\int_0^{1}\left\langle b_1 w^{*}, v-w^{*}\right\rangle_{L^2(\Omega)} dt.$$

Considering that

$$\begin{aligned} \int_0^{t_f}\langle D\psi, DZ\rangle dt &= \int_0^{t_f}\left\langle D^{*}D\psi, Z\right\rangle dt \\ &= \int_0^{t_f}\left\langle -\frac{\partial q}{\partial t}-Aq-F^{*}q, Z\right\rangle dt \\ &= \int_0^{t_f}\left\langle q, \frac{\partial Z}{\partial t}-AZ-FZ\right\rangle dt \\ &= \int_0^{t_f}\langle q, B(v-w^{*})\rangle\, dt \\ &= \int_0^{t_f}\left\langle B^{*}q, v-w^{*}\right\rangle_{L^2(\Omega)} dt, \end{aligned}$$

and since W_{ad} is convex, we have $C'\left(w^{*}\right)\left(v-w^{*}\right)\geq 0$ for every $w\in W_{ad}$, which is equivalent to

$$\int_0^{t_f}\left\langle B^{*}q+b_1 w^{*}, v-w^{*}\right\rangle_{L^2(\Omega)} dt\geq 0 \text{ for every } w\in W_{ad}.$$

Thus, $bw^{*}=-B^{*}q$, which implies $w^{*}=\frac{(q_2-q_1)\beta z_1^{*}z_2^{*}}{b_1}$. Given that $w^{*}\in W_{ad}$, it follows that (38) holds.

This result is important as it provides the explicit form of the optimal control u^{*} in terms of the adjoint variables q_1 and q_2, as well as the state variables z_1^{*}, z_2^{*}, and z_3^{*}. This formulation allows for a deeper understanding of the interaction between the state and adjoint systems in the context of the optimal control problem. The conditions under which this optimal control is

derived ensure that the solution is both feasible and optimal within the given constraints. □

6 Computational modeling and outcome display

To accomplish the objectives of optimal control and evaluate the precision of our spatio-temporal model, both with and without control interventions, we executed a numerical simulation of our optimal control problem within the realm of disease spread modeling. This study adopts a stringent methodological framework. Our optimality system is delineated by state equations with initial and boundary conditions (2)-(4), adjoint equations with transversality conditions (36), and an optimal control formulation (38). To resolve this system, we employ the forward-backward scanning method in an iterative manner. Temporal discretization of the state equations is performed using the explicit Euler method, while the adjoint equations are solved retrospectively. The spatial domain considered, symbolizing a city $\Omega = 75\,\mathrm{Km}^2$, is initially populated randomly at $t = 1$ day, under the assumption that the epidemic commenced spreading randomly across various sections of the city. The outcomes will be delineated as follows.

To deepen our understanding, we performed additional simulations to evaluate the impact of various control strategies on disease dynamics. These simulations offer further insights into the effectiveness of different intervention measures under various scenarios, enhancing the robustness of our model. The data and results obtained from these simulations will be meticulously analyzed and discussed to provide comprehensive insights into the model's performance under different conditions.

The parameter values associated with our spatio-temporal model, with and without control measures, are presented in Table 3 below.

Figure 2 reveals that before the imposition of control measures, asymptomatic infections were prevalent throughout numerous locations in the region. This observation implies a broad dissemination of the epidemic within the city. Furthermore, Figure 4 depicts a consistently high proportion of asymptomatic cases, sustaining a steady rate of 13% of the total population over time. This continuous presence of asymptomatic individuals facilitated

Table 3: Model parameters in scenarios with and without control measures.

Parameters	Values
$(\Sigma, \mu, \alpha, \beta, \lambda, \gamma, \theta)$	(0.07,0.12,0.75,0.5,0.0002,0.001,0.03)
$(d_S, d_E, d_I, d_Q, d_R)$	(0.25,0.25,0.25,0.25,0.25)

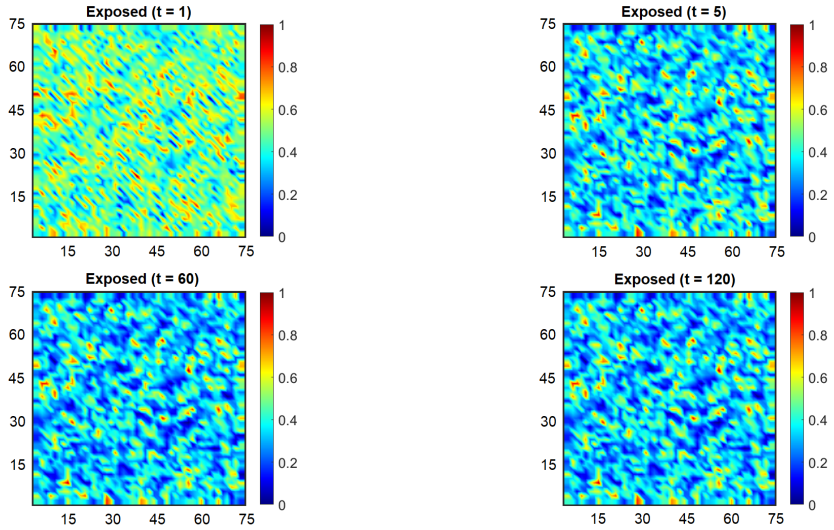

the emergence of a substantial cluster of symptomatic cases across the city, representing 34% of the total population. The visual representation underscores the extensive transmission of the infection in various areas within the city.

Furthermore, the data reveals that the uncontrolled spread of asymptomatic infections is a key factor in the rapid escalation of the epidemic. This situation underscores the importance of early intervention and the implementation of control measures to curb the virus's spread. The figures collectively provide a clear illustration of how the infection permeated various sections of the city, resulting in a substantial number of symptomatic cases and emphasizing the necessity for timely and effective public health responses.

To elaborate further, the persistence of asymptomatic cases not only increased the number of symptomatic individuals but also placed a strain on

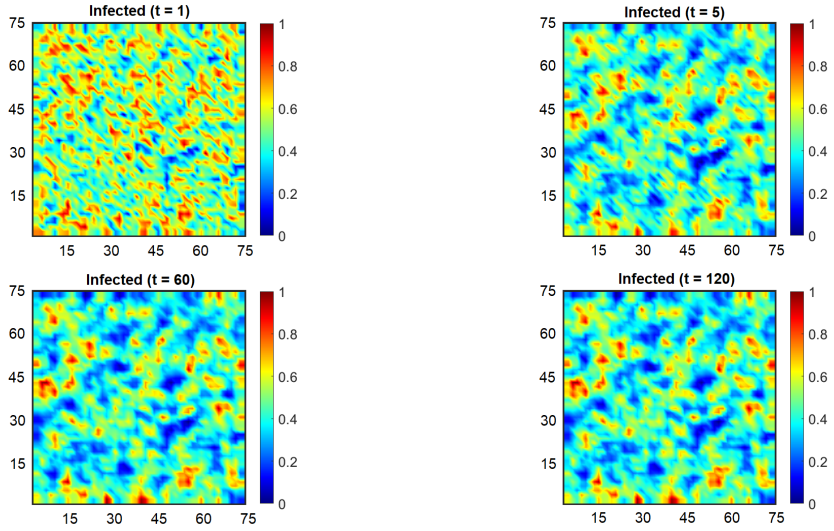

Figure 2: The dynamics of compartments E and I in the absence of control measures

the healthcare system. The widespread nature of the infection required urgent and comprehensive measures to control its transmission. The figures thus provide valuable insights into the dynamics of disease spread and the critical need for strategic interventions.

Figure 3 illustrates a significant shift in the epidemic landscape following the implementation of stringent control measures. These carefully planned interventions aimed to drastically reduce the widespread incidence of asymptomatic infections across the region. Key elements of these measures included limiting social interactions, launching safety campaigns to discourage migration, and promoting health precautions to reduce virus transmission. As depicted in Figure 4, these proactive efforts led to a dramatic decrease in the overall percentage of asymptomatic cases, dropping from an initial 13% to just 0.25%. Consequently, there was a marked decline in the number of symptomatic cases, with the affected population now representing only 0.3% of the total. This positive outcome highlights the effectiveness of the control measures in curbing the spread of the disease and reducing its impact on the population. The resulting scenario reflects a more controlled and manageable situation, underscoring the success of the interventions in limiting the transmission of the infection within the city.

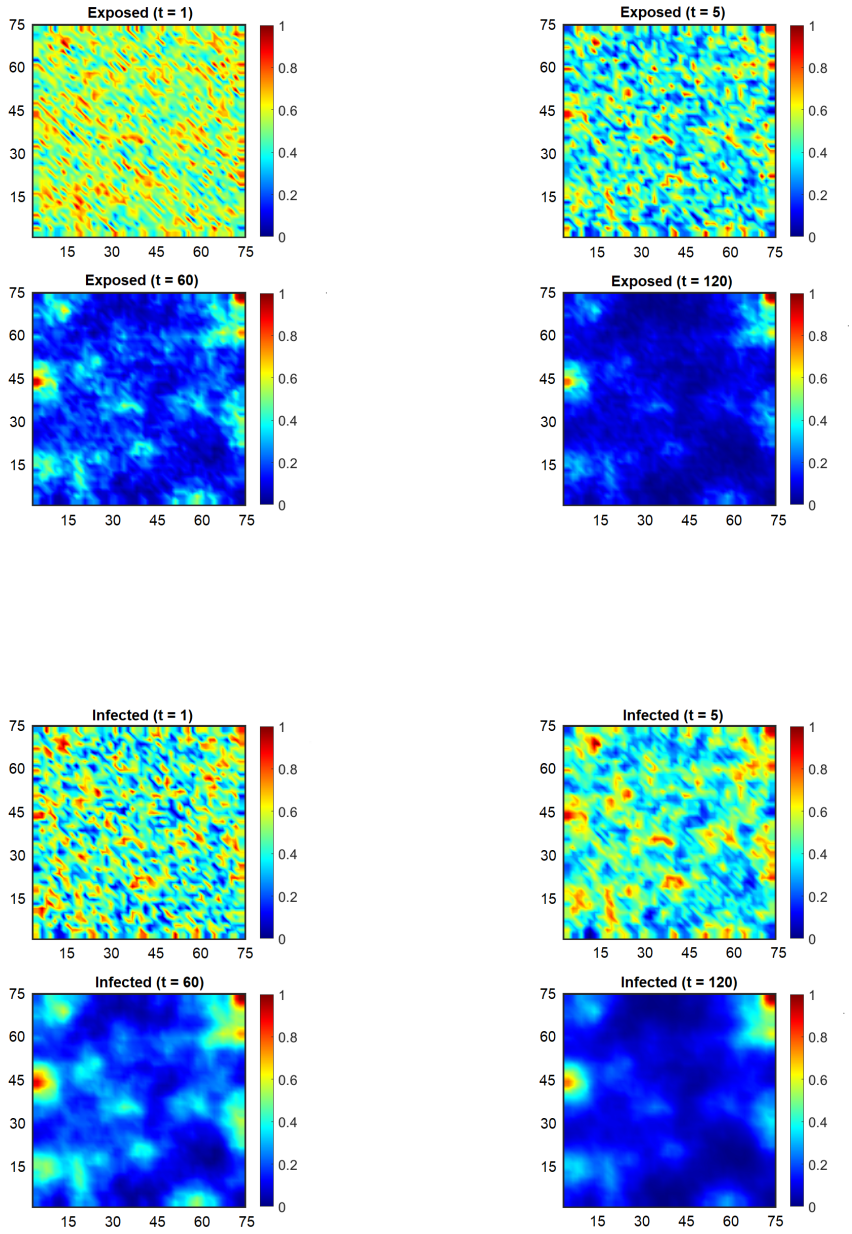

Figure 3: Dynamics of compartments E and I under the influence of control measures

Furthermore, the findings underscore the importance of timely interventions in managing the epidemic. The substantial reduction in both asymptomatic and symptomatic cases demonstrates the significant impact of early and decisive action. These control measures not only slowed the spread of the virus but also eased the burden on the healthcare system, allowing it to operate more efficiently and effectively.

In addition, the data suggests that ongoing monitoring and adjustment of control strategies are essential to maintaining the low infection rates that have been achieved. The evolving nature of the epidemic requires adaptive response measures to address new challenges as they emerge. This approach ensures sustained control over the virus, helping to prevent future outbreaks and ultimately protecting public health and well-being.

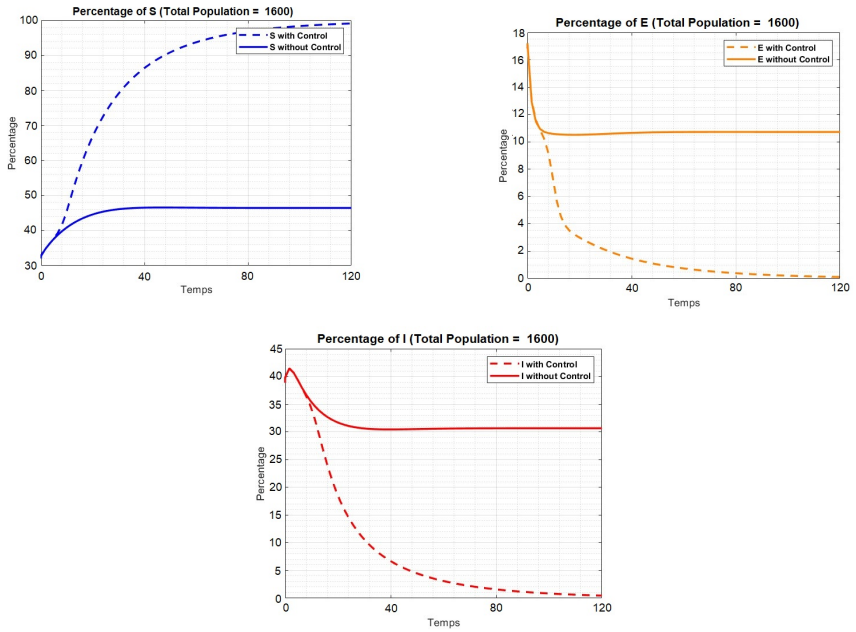

Figure 4: The proportional distribution of compartments S, E, and I in relation to the total population

7 Conclusion

The spatio-temporal model employed in this investigation adeptly encapsulates essential elements such as population density, movement trajectories, and social interactions, which are paramount for comprehending the transmission dynamics of the MPX virus. Our research underscores the critical importance of control measures via diverse intervention strategies, including advocacy campaigns, the creation of social barriers, and targeted testing, to thwart the virus's proliferation while mitigating associated costs and societal upheavals.

Moreover, our examination of this spatio-temporal epidemiological model makes a substantial contribution to the decision-making process and elucidates fundamental mechanisms in epidemic progression. This methodology has the potential to amalgamate rigorous mathematical analysis with empirical data to discern effective targeted therapies, thereby bolstering global endeavors to combat the virus and safeguard public health.

To further refine the accuracy and effectiveness of these models, future iterations should incorporate additional variables such as age, socio-economic status, and behavioral patterns. Enhancing data collection frameworks and developing comprehensive reports will yield current, reliable data for precise sampling, which is indispensable for informing efficacious epidemic mitigation strategies.

Moreover, integrating advanced computational techniques and machine learning algorithms could further refine the model's predictive capabilities. This integration would enable more nuanced simulations and better preparedness for potential future outbreaks. Collaborative efforts across various disciplines, including epidemiology, data science, and public health, will be essential to develop and implement these sophisticated models.

In conclusion, the continuous evolution and refinement of spatio-temporal models are essential for addressing the complex dynamics of epidemic spread. By leveraging these advanced tools, we can enhance our understanding and management of infectious diseases, ultimately safeguarding human health on a global scale.

Acknowledgements

Authors are grateful to there anonymous referees and editor for their constructive comments.

Conflicts of interest

The authors declare no conflicts of interest.

References

[1] Amaral, A.V.R., González, J.A. and Moraga, P. *Spatio-temporal modeling of infectious diseases by integrating compartment and point process models*, Stoch. Environ. Res. Risk Assess. 37 (4) (2023) 1519–1533.

[2] Barbu, V. *Mathematical methods in optimization of differential systems*, Vol. 310: Springer Science and Business Media, 2012.

[3] Baroudi, M., Gourram, H., Labzai, A. and Belam, M. *Mathematical modeling and Monkeypox's optimal control strategy*, Commun. Math. Biol. Neurosci. 2023 (2023) Article ID 110.

[4] Bleichrodt, A., Dahal, S., Maloney, K., Casanova, L., Luo, R. and Chowell, G. *Real-time forecasting the trajectory of Monkeypox outbreaks at the national and global levels, July–October 2022*, BMC Med. 21 (1) (2023) 19.

[5] Bourdaud, G. *Le calcul fonctionnel dans les espaces de Sobolev*, Séminaire Équations aux dérivées partielles (Polytechnique) dit aussi Séminaire Goulaouic-Schwartz (1991) 1–4.

[6] Chen, D., Moulin, B. and Wu, J. *Analyzing and modeling spatial and temporal dynamics of infectious diseases*: Wiley Online Library, 2015.

[7] Falb, P.L. and Athans, M. *Optimal control: An introduction to the theory and its applications*, Dover Publications, 2006

[8] Gérard, P. *Description du défaut de compacité de l'injection de Sobolev*, ESAIM: Contr. Optim. Calculus Var. 3 (1998) 213–233.

[9] Hoff, N.A., Doshi, R.H., Colwell, B., Kebela-Illunga, B., Mukadi, P., Mossoko, M., Muyembe-Tamfum, J.J., Okitolonda-Wemakoy, E., Lloyd-Smith, J. and Rimoin, A.W. *Evolution of a disease surveillance system: an increase in reporting of human Monkeypox disease in the Democratic Republic of the Congo, 2001–2013*, Int. J. Trop. Dis. Health, 25 (2) (2017).

[10] Islam, M.A., Sangkham, S., Tiwari, A., Vadiati, M., Hasan, M.N., Noor, S.T.A., Mumin, J., Bhattacharya, P. and Sherchan, S.P. *Association between global Monkeypox cases and meteorological factors*, Int. J. Environ. Res. Public Health, 19 (23) (2022) 15638.

[11] Liu, B., Farid, S., Ullah, S., Altanji, M., Nawaz, R. and Wondimagegnhu Teklu, S. *Mathematical assessment of Monkeypox disease with the impact of vaccination using a fractional epidemiological modeling approach*, Sci. Rep. 13 (1) (2023) 13550.

[12] Mandja, B.A.M., Brembilla, A., Handschumacher, P., Bompangue, D., Gonzalez, J.P., Muyembe, J.J. and Mauny, F. *Temporal and spatial dynamics of Monkeypox in Democratic Republic of Congo, 2000–2015*, EcoHealth 16 (2019) 476–487.

[13] Moumine, E.M., Balatif, O. and Rachik, M. *Mathematical analysis and forecasting of controlled Spatio-temporal dynamics of the EG. 5 virus*, Iranian Journal of Numerical Analysis and Optimization 14 (2) (2024) 500–521.

[14] Munir, T., Khan, M., Cheema, S.A., Khan, F., Usmani, A. and Nazir, M. *ime series analysis and short-term forecasting of Monkeypox outbreak trends in the 10 major affected countries*, BMC Infect. Dis. 24 (1) (2024) 16.

[15] Ozoliņš, V., Lai, R., Caflisch, R. and Osher, S. *Compressed plane waves yield a compactly supported multiresolution basis for the Laplace operator*, Proc. Natl. Acad. Sci. 111 (5) (2014) 1691–1696.

[16] Pal, M., Mengstie, F. and Kandi, V. *Epidemiology, diagnosis, and control of Monkeypox disease: A comprehensive review*, Am. J. Infect. Dis. Microbiol. 5 (2) (2017) 94–99.

[17] Rodriguez, N. and Bertozzi, A. *Local existence and uniqueness of solutions to a PDE model for criminal behavior*, Math. Models Methods Appl. Sci. 20 (supp01) (2010) 1425–1457.

[18] Smouni, I., El Mansouri, A., Khajji, B., Labzai, A., Belam, M. and Tidli, Y. *Mathematical modeling and analysis of a Monkeypox model*, Commun. Math. Biol. Neurosci. 2023 (2023) Article ID 85.

[19] Stengel, R.F. *Optimal control and estimation:* Courier Corporation, 1994.

[20] Takhar, S.S. *Epidemiologic and clinical characteristics of Monkeypox cases–United States, May 17-July 22, 2022*, Ann. Emerg. Med. 81, (1) (2023) 31–34.

[21] Talisuna, A.O., Okiro, E.A., Yahaya, A.A., Stephen, M., Bonkoungou, B., Musa, E.O., Minkoulou, E.M., Okeibunor, J., Impouma, B., Djingarey, H.M. and YAO, N.D.K.M. *Spatial and temporal distribution of infectious disease epidemics, disasters and other potential public health emergencies in the World Health Organisation Africa region, 2016–2018*, Glob. Health. 16 (2020) 1–12.

[22] Wittenberg, R.W. *Local dynamics and spatiotemporal chaos. The Kuramoto-Sivashinsky equation: A case study*, Princeton University, 1998.

[23] Yang, S. *Global solutions of nonlinear wave equations with large data*, Sel. Math. 21 (2015) 1405–1427.

[24] Yinka-Ogunleye, A., Aruna, O., Dalhat, M., Ogoina, D., McCollum, A., Disu, Y., Mamadu, I., Akinpelu, A., Ahmad, A., Burga, J. and Ndoreraho, A., *Outbreak of human Monkeypox in Nigeria in 2017–2018: a clinical and epidemiological report*, Lancet Infect. Dis. 19 (8) (2019) 872–879.

[25] Zebardast, A., Latifi, T., Shafiei-Jandaghi, N.Z., Gholami Barzoki, M. and Shatizadeh Malekshahi, S. *Plausible reasons for the resurgence of Mpox (formerly Monkeypox): An overview*, Trop. Dis. Travel Med. Vaccines. 9 (1) (2023) 23.